Production of lightweight expanded aggregates from smectite clay, palygorskite rich-sediment and phosphate sludge

Sameh Jaha[1*], João Carvalheiras[2], Salah Mahmoudi[1], João Labrincha[2]

[1] Research Laboratory of Geo-systems, Geo-resources and Geo-environments (LR3G), Department of Earth Sciences, Faculty of Sciences of Gabes (FSG), University of Gabes, 6072, Zrig, Gabes, Tunisia

[2] Department of Materials and Ceramic Engineering / CICECO-Aveiro Institute of Materials, University of Aveiro, Campus of Santiago, 3810-193, Aveiro, Portugal

* Corresponding author: samah.jahha@yahoo.com

* Research Laboratory of Geo-systems, Geo-resources and Geo-environments (LR3G), Department of Earth Sciences, Faculty of Sciences of Gabes (FSG), University of Gabes, 6072, Zrig, Gabes, Tunisia

Submitted: 1 December 2023. Revised: 27 March 2024. Associate editor: M. Dondi.

Abstract-Lightweight expanded clay aggregates (LWAs) are porous materials with low density and lofty strength (UNE-EN-13055-1), important in sustainable construction to assure lightness and thermal or acoustic insulation. The objective of this work was therefore to evaluate the preparation of LWAs using a smectite clay (formulation M1), whose use in common ceramic production is difficult. An alternative approach was proposed for the valorization of phosphate sludge and a palygorskite-rich sediment, by mixing them with expanded clay (M2 formulation) for LWAs production. This should result in economically cost-effective products with significant environmental benefits. Pellets were prepared and fired at different temperatures (1100°C, 1125°C and 1150°C), and relevant properties like bloating index, density, water absorption and compressive strength were determined. Additionally, the microstructure, mineralogical transformations and phase compositions under different sintering temperatures were investigated. As a result, increasing temperature from 1000 to 1150°C

DOI: 10.1180/clm.2024.10

improves significantly the expansion properties of LWAs, and 1150°C seems the optimal firing temperature at which, the best expansion properties were achieved. In addition, the incorporation of the selected waste improves the properties of the final products leading to lower density, higher strength and higher bloating with the development of the internal pore structure as compared to the LWAs without addition. Because of their low density (0.6 g/cm^3) and sufficient compressive strength (0.86 MPa), the manufactured lightweight aggregates can be used in construction (as insulating panels or in lightweight concrete), and in green roofs.

Keywords: smectite clay, palygorsikte rich-sediment, phosphate sludge, lightweight aggregates, density, microstructure.

INTRODUCTION

Light weight aggregates (LWAs) are granular materials with a well developed pore structure and a bulk density lower than 1.2 g/cm^3 **(González-Corrochano et al., 2011, Soltan et al., 2016)**. In general, the quality of obtained products depends on the chemical and mineralogical characteristics of the raw materials and on the firing process. Usually, LWAs are obtained at temperatures 900-1250°C, and soaking time 3-30 minutes depending on the kiln type (muffle furnaces or rotary kilns) **(González-Corrochano et al., 2011; Loutou et al., 2013; Volland et al., 2015, Liu et al., 2017; Moreno-Maroto et al., 2017; Ayati et al., 2018; Sun et al., 2021, Li et al., 2021)**. Recent lab-scale studies report the use of microwave radiation for the production of LWAs **(Franus et al., 2019)**. Clays are the most common raw materials used for LWAs production, especially plastic clays such as smectite and vermiculite, due to their plasticity (to facilitate pellet shaping), and chemical and mineralogical composition (presence of decomposable components that generate gases upon firing, such as carbonates, organic matter and iron oxide) **(Ayati et al., 2018)**. In Tunisia, only few studies have been conducted on the preparation and characterization of raw clays, from the south of the country, in LWAs production **(Fakhfakh et al., 2007)**. The results showed that some clays are suitable for producing low dense products, without or with quartz addition depending on the sintering temperature.

Palygorskite is a naturally occurring fibrous clay mineral of sedimentary origin, member of the sepiolite-palygorskite group of minerals. It is generally neoformed in soils and paleosols under dry or semi-dry climates **(Da Silva et al., 2018)**. Chemically, palygorskite is a fibrous hydrated magnesium-aluminium silicate with a micro-channel structure and with typical chemical

https://doi.org/10.1180/clm.2024.10 Published online by Cambridge University Press

formula $Si_8\ O_{20}\ (Mg,Al,Fe)_5\ (OH)_2\ (OH_2)_4\ 4H_2O$, **(Zhao et al., 2006; Suárez and García-Romero, 2011)**. Palygorskite has a wide range of industrial applications in particular for fiberglass, nanocatalysts, plasters, rubbers and agriculture **(Murray, 2000 and Alvarez et al., 2011)**. Due to its sorptive, rheological and catalytic properties, palygorskite has been used as supporting material for the preparation of a wide variety of nanocomposites, membranes and coatings **(Zhang et al., 2016; Ezzatahmadi et al., 2019; Lakbita et al., 2019; Wang et al., 2016; Wei et al., 2019; Chen et al., 2021, Fan et al., 2021)**. Recently, palygorskite has also been used in bricks production **(Loutou et al., 2019; Zhang et al., 2019; Fan et al., 2021; Wang et al., 2022)**. There are a few studies **(Frayyeh et al., 2014; Moreno-Maroto et al, 2020)** reporting the use of palygorskite in LWAs manufacturing. **Frayyeh et al. (2014)** tested the production of LWAs based on an Iraqi palygorskite clay, by firing at 1100°C for 30min, that yielded materials with relatively low density (808 kg/m^3). In addition, **Moreno-Maroto et al. (2020)** suggested that a clay material having smectite and palygorskite as major components (Portuguese clay) has suitable bloating ability when sintered at 1210°C for 4 minutes. Obtained pellets showed good technological properties, namely low density and high compressive strength.

LWAs might be successfully manufactured by using various industrial by-products and waste as substitutes of natural raw materials. Examples include the use of automotive plastics **(Liu et al., 2017)**, wastewater sludge **(Mañosa et al., 2021)**, bauxite tailings **(Yang et al., 2022)**, waste glass **(Liu et al., 2022, Graziano et al., 2022)**, granite sawing waste **(Soltan et al., 2016)**, petrochemical waste **(Juan Daniel Martinez et al., 2018)**, and phosphate by-products or waste **(Loutou et al., 2013; Bayoussef et al., 2021a; Chao Ding et al., 2022)**. Phosphate sludge, in particular, is a by-product of phosphate beneficiation, the production of which will increase in the next years. South of Tunisia is one of the places where phosphate sludge has been stockpiled in huge quantities, so that new recycling solutions are critically required to reduce economic and environmental impacts. Some studies report the reuse of phosphate sludge in geopolymers and in ceramic formulations (e.g., bricks) **(Mabroum et al., 2020, Moukannaa et al., 2019; Loutou et al., 2019; Bayoussef et al., 2021b; Dabbebi et al., 2018; Ettoumi et al., 2021)**. However, few studies focus on the reuse of phosphate sludge for the production of LWAs **(Loutou et al. 2013)**. These authors confirm that the incorporation of phosphate sludge is beneficial, since it can act as pore-forming or gas-releasing agent after decomposition of some inherent compounds.

https://doi.org/10.1180/clm.2024.10 Published online by Cambridge University Press

This paper investigates the production of low density and porous LWAs using smectite clay as the main raw material, palygorskite rich-sediment and phosphate sludge as additives, and the firing process was studied in an attempt to assure maximum bloating and to develop a porous structure. The produced LWAs were characterized to inspect their mineralogical, physical-mechanical and microstructural properties, and the relevant formation mechanism of internal structure in the prepared LWAs were examined. The objective of using smectite clays results from its expandable characteristics during firing, and the addition of phosphate sludge and palygorskite rich-sediment could help to improve some properties such as porosity, density, water absorption and compressive strength of the LWAs. Also, the recycling of such wastes/by-products has an obvious environmental impact, contributing to the circular economy.

MATERIALS AND METHODS

Materials

The raw materials used in this work were a smectite clay (SmC), a palygorskite rich-sediment (PalS) and phosphate sludge (PhS). The M1 was formulated only with SmC and the M2 mixture was prepared by mixing 50% SmC, 25%PalS and 25%PhS. This formulation was chosen after several laboratory tests in which different mixtures with different proportions of PhS and PalS additions, were used (Table1).

The clay was collected on the El Hamma region in Gabes governorate, SE Tunisia. It belongs to the Upper Cretaceous sedimentary clayey series (Coniacian-Santonian), exposed for over 35 km in a roughly NE–SW direction along the Northern Chotts chain in southern Tunisia, which has significant reserves of smectitic clays **(Boussen et al., 2015)**. These clays were used on phosphoric acid purification **(Trabelsi et al., 2017)**. The palygorskite rich-sediment is part of vast alluvial deposits occurring also in Gabes region, South Tunisia. Despite the large reserves, its industrial use has never been developed to date due to its heterogeneous mineralogical and chemical composition and abundant impurities. The use of this raw material for LWAs might constitute an innovative approach. The phosphate sludge was collected from the Metlaoui phosphate plant located in Gafsa mining district, South Tunisia. During beneficiation, fluorapatite is separated from associated gangue minerals by crushing, screening, washing, and flotation. This treatment generates large volume of waste, mostly phosphate sludge, which is stockpiled in tailings ponds within the processing plant.

https://doi.org/10.1180/clm.2024.10 Published online by Cambridge University Press

Characterization techniques

All the characterization techniques were carried out in the laboratories of the Materials and Ceramics Engineering Department at the University of Aveiro in Portugal and in the research laboratory Geosystems, Georesources and Geoenvironments in the Faculty of Sciences of Gabes, University of Gabes in Tunisia.

X-ray fluorescence spectroscopy (XRF, Philips X'Pert Pro MPD) was used to determine the chemical composition of the raw materials and the loss on ignition (LOI) which corresponds to the weight loss of a sample after heating to 1000°C.

X-ray diffraction (XRD) analysis was used to determine the mineralogical composition of the raw materials. A Panalytical X'PERT PRO^3 XRD was utilized, CuKα radiation 40 A and 45 kV. The mineralogical composition of the bulk materials was determined using powder XRD. The XRD traces were recorded between 3–70°2θ at a step size of 0.017°2θ. The mineralogical composition of the clay fraction was determined with oriented slides. Carbonates and organic matter were eliminated prior to the separation of the clay fraction by centrifugation. Suspensions were placed on glass slides, the standard tests after air-drying, saturated with ethylene glycol and heated at 550°C. The XRD traces of clay fractions were obtained from 2 to 30°2θ. Mineral phase identification was carried out using the X'pert High Score plus software.

The particle size distribution was analyzed by laser diffraction in the range 0.04 mm - 2000 mm with a Coulter LS230 equipment. The plasticity was evaluated through determination of Atterberg limit on a fraction below 400µm. Liquid limit (LL) was determined using Casagrande method, while the plastic limit (PL) was estimated by repeated rolling of an ellipsoidal-sized sample mass by hand on a flat surface. The plasticity index (PI) was determined form the difference between LL and PL values.

Simultaneous Differential Scanning Calorimetry-Thermogravimetric Analysis (DSC-TGA) was used to investigate the thermal behavior of raw materials. This technique allows measuring both heat flow and weight changes in a material as a function of temperature in a controlled atmosphere. The obtained results allow differentiation between endothermic events which involve a weight loss and exothermic events without associated weight loss. The DSC-TGA analyses were performed with a HITACHI STA300 coupled device, reaching a maximum temperature of 1200 °C, in inert atmosphere at a heating rate of 5°C min^{-1}, using α-Al_2O_3 as an inert material.

https://doi.org/10.1180/clm.2024.10 Published online by Cambridge University Press

Preparation of pellets and firing process

The production of LWAs involved three main steps, namely the preparation of powders and mixtures formulation, pelletization and firing (Fig. 1). The first step involved drying the constituents at 105°C for 24 hours to assure removal of free water. Then, materials were crushed in a jaw crusher and sieved through a 200 μm sieve. The preparation of the raw material was carried out according to **Moreno-Maroto et al. (2020)**. After weighing, powders were moistened and hand mixed to get a homogeneous sample so that was shaped as small pellets with diameter between 12 and 15 mm. The pellets were dried at room temperature for 72 hours, then at 115°C for 48 hours until constant weight. The firing process, conducted in a lab-scale muffle furnace (Fig. 1) was critically studied, attempting to adjust the heating rate, maximum temperature and soaking time. After several trials, the following conditions were defined: (i) firing temperatures 1100°C, 1125°C and 1150°C; (ii) heating rate of 5°C/min; (iii) soaking time 15 minutes followed by fast cooling.

LWAs properties characterization

The crystalline phases formed upon firing were identified by X-ray diffraction, in the same conditions as previously described. The microstructure, was examined by scanning electron microscopy (SEM, Hitachi S4100 and Quanta 250 equipped with energy dispersion spectroscopy, EDS). The shell part of LWAs and their interior structure were observed and compared. Energy Dispersive Spectrometry (EDS) analysis was conducted to analyze the elemental composition and distribution (EDS mapping) of the LWA matrix.

The bloating index (BI) expresses the volume change after sintering of the LWAs. It was determined according to **González-Corrochano et al. (2011)** using the following equation:

$$BI\ (\%) = \frac{D2-D1}{D1} * 100 \qquad [1]$$

Where D1 and D2 are the diameters of pellets before and after sintering, respectively.

The bulk density was determined using the sand dislocation method, (**De Jesus Fernandes Pinto, 2005)**. Each test was repeated and the average value was determined.

The water absorption of the pellets after 24 h immersion in water, was determined using the standard **UNE-EN-1097-6 (2013)**, according to equation [2]:

$$WA\ (\%) = \frac{M2-M1}{M1} * 100 \qquad [2]$$

M1: is the mass (g) of saturated pellets, after immersion in water

https://doi.org/10.1180/clm.2024.10 Published online by Cambridge University Press

M2: is the mass (g) of the dry pellets, before immersion in water.

The compressive strength (CS) of sintered LWAs was evaluated based on the load of rupture measured by pressing with a maximum pressure of 5 kN, and a loading rate of 0.5 mm/min using a sphere uniaxial compressive machine. The compressive strength was calculated using the determined rupture load values according to the following equation **(Moreno-Maroto et al., 2020)**:

$$\sigma c(\mathrm{MPa}) = \frac{2.8\mathrm{Fc}}{\pi \mathrm{D}^2} \quad [3]$$

where Fc is the rupture load (N) and D is the diameter of sintered pellets (mm).

RESULTS AND DISCUSSION

Raw materials characterization

Chemical composition

The chemical compositions of the used raw materials (SmC, PalS and PhS) (Table 2) show that the smectite clay (SmC) is characterized by high contents of SiO_2 (51.55%), Al_2O_3 (13.28%) and Fe_2O_3 (6.67%). The CaO, MgO, K_2O, Na_2O and SO_3 amounts are relatively low and may be related to the presence of minor quantities of calcite, dolomite, feldspars, and gypsum. This composition is comparable to that of some other clays used for the production of LWAs **(Liu et al., 2017, Anan et al., 2017, Moreno-Maroto et al, 2020; Abdelfattah et al., 2022)**. The main oxides in the PalS sample were SiO_2 (34.11%), Al_2O_3 (8.94%) and CaO (22.04%), with Fe_2O_3 (4.03%), MgO (3.39%) SO_3 (8.43%) being also abundant. The phosphate sludge (PhS) is mainly composed of CaO (31.29%), SiO_2 (21.88%) and P_2O_5 (16.72%), that are related to the raw phosphate rock composition, which is rich in carbonate-fluorapatite **(Ettoumi et al., 2020)**. Other oxides, including Al_2O_3 (3.8%), SO_3 (3.73%), MgO (2.01%) and F (1.34%), are present in minor amounts. All studied materials show high LOI, namely 16.8%, 15.84% and 15.62% for SmC, PalS and PhS respectively. The LOI is mainly due to the dehydroxylation of clay minerals, organic matter oxidation and decomposition of carbonates and hydroxides with release of water vapor and various gases during firing (**Abdelmalek et al., 2017**),

Mineralogical composition

https://doi.org/10.1180/clm.2024.10 Published online by Cambridge University Press

Figure 2a presents the XRD traces of Smc, PalS and PhS bulk samples while Figure 2b displays the XRD traces of the oriented clay samples. The semi-quantitative estimation of the main crystalline phases (Table 3) shows that the main mineral phases identified in the SmC sample are mainly smectite (montmorillonite) as major clay mineral and quartz as major associate mineral with minor calcite and gypsum. Similar XRD data were reported by **Boussen et al. (2015)**, confirming the presence of the (001) diffraction plane (at 14.5 - 15 Å) of montmorillonite.

The PalS consists mainly of palygorskite in addition to quartz, calcite, dolomite and gypsum as associated minerals. Palygorskite is often present in some Tunisian clay-rich sediments as a fibrous clay mineral characterized by its (001) diffraction peak at 10.5 Å **(Tlili et al., 2010)**. Similar results have been reported in recent work of **Saadaoui and Eloussaief (2017)** and **Allouche et al. (2020)**.

The main mineral phases of phosphate sludge are fluorapatite, quartz, calcite, dolomite, gypsum and smectite, in accordance with **Ettoumi et al. (2020)**. The presence of these phases is associated to the fine and undesirable fractions eliminated after the washing of the phosphates.

The XRD traces of clay fractions (Fig. 2b) demonstrate that the dominant mineral is smectite in SmC sample and palygorskite in PalS sample with minor amounts of illite (9.99 Å) and kaolinite (7.16 Å). Therefore, the reflection intensity of 14.48 Å in air-drying test is associated with the presence of 2:1 mineral. This peak shifted to 17.8 Å after saturation with ethylene glycol, and to 10 Å after heating at 550 °C, being typical of smectite. The peak at 10.48 Å in air drying preparations the first-order peak of palygorskite, and the peak at 6.37 Å is associated with the second-order peak of this mineral. The peaks were not affected by ethylene glycol treatment confirming the presence of palygorskite.

Particle size distribution and plasticity

The particle size distributions of the raw materials (Fig. 3) and the relevant features (Table 4), reveal that SmC and PalS exhibit narrow distributions with particle sizes between 0.1 and 50 µm. The PhS shows a wider size distribution, with particle sizes reaching 110 µm. The clay fraction content (< 2 µm) was about 40% in SmC, 8% in PalS, and about 10% in PhS. These results agree with the nature and mineralogy of the materials. The silt fractions (2-63

https://doi.org/10.1180/clm.2024.10 Published online by Cambridge University Press

μm) were 60%, 92%, and 42% in SmC, PalS, and PhS, respectively. Both PalS and SmC lack sand fraction (ø > 63 μm) but PhS contains ~ 48% sand fraction.

The particle size plays an important role in plasticity, since this property is associated with the clay fraction of the material **(Moreno-Maroto et al., 2020)**. The results of the Atterberg limits (Table 3) show that the studied materials have moderate to high liquid limits: 64% for SmC and 52% for PalS, with plasticity indices of 32% and 39%, respectively. These moderate to high values are usually attributed to the presence of montmorillonite in SmC and palygorskite in PalS (**Daoudi et al., 2015; Abbaslou et al., 2016)**.

Thermal analysis

Figure 4 shows the thermal analysis curves (DSC_DTG) of studied materials. The DSC-TG curve of SmC show the presence of three endothermic and one exothermic event, with a total weight loss of about 18.5% up to 1150°C (Fig. 4a). This value is in accord with the LOI determination. The first endothermic event occurs between 50 and 250°C and involves an significant weight loss of ~ 14%, mainly due to the removal of adsorbed and interlayer water, in agreement with **Alabarse et al. (2011)** and **Arab et al. (2015)**.

The second weight loss event was observed in the 400-600°C range and is mainly due to the dehydroxylation of clay minerals, with an endothermic peak above 500°C and a weight loss of ~ 4%. The obtained results are in accord with **Fontaine et al. (2020)**. This confirms that the studied clay (SmC sample) is a Fe-Smectite as shown by the chemical analysis. According to **Arab et al. (2015)**, dehydroxylation occurs between 400°C and 700°C, with Fe-rich smectites showing an endothermic peak at approximately 500°C, while Fe-poor smectites show the same peak at approximately 700°C. The third step occurred at approximately 850°C with a small weight loss < 1% due to carbonates decomposition. The single exothermic event occurs near 1000°C without weight loss and is related to recrystallization **(Mahmoudi et al., 2017; Chalouati et al., 2020)**.

The DSC-TG curves of the PalS sample (Fig. 4b) show four events, similar to those observed by **De Souza et al. (2021)** and **Wang et al. (2021)**. The first event involves a strong endothermic peak, centered at about 120 ºC with weight loss of ~10%, due to the removal of adsorbed water and zeolitic water from palygorskite channels. The second event is observed between 400-600°C with an endothermic peak at about 500°C and a weight loss of 3.5%, due to the removal of zeolitic water.

https://doi.org/10.1180/clm.2024.10 Published online by Cambridge University Press

The third event occurs between 700 and 900°C with an endothermic peak at 750°C and a relative weight loss of 8.5%. This is mainly due to carbonates decomposition **(Karunadasa et al., 2019)** and dehydroxylation of palygorskite, which occurs between 700 and 900°C **(Wang et al., 2022 and Frost and Ding 2003)**, jointly present in the PalS sample as was confirmed by XRD. This last endothermic peak is immediately followed by a broad exothermic peak coinciding with the structural collapse of palygorskite, as well as the possible phase recrystallization.

The DSC-TG curves of phosphate sludge (PhS) exhibit four successive endothermic events, due to the presence of clay minerals, carbonates and phosphates in the sample (Fig. 4c). The first event extends from room temperature to 200°C with a weight loss of 3.5%, which corresponds to the removal of adsorbed water. The second event, due to the dehydration, occurs between 200°C and 500°C with a weight loss of 3%. The third event is observed between 400°C and 650°C and is assigned to the dehydroxylation of clay minerals. The last loss occurs between 650°C and 900°C, with a large endothermic peak centered near 750ºC and a total weight loss of 9%, due to the decomposition of calcite. Finally, an exothermic event without mass loss is observed at ~ 1000°C and is assigned to the Ca-Mg-silicates formation (**Harech et al. 2021, 2022)**.

Characterization of lightweight aggregates

XRD analysis

The XRD traces of the LWAs sintered at 1100, 1125 and 1150°C show significant phase changes (Fig. 5). As expected, the firing caused changes in the initial crystalline phases. The clay minerals (smectite and palygorskite) underwent transformations while carbonates, mainly calcite and dolomite, decomposed in agreement with thermal analyses. Quartz which was initially present in the raw clays was identified in the M1 and M2 pellets. The peak intensity of quartz decreases with the increasing temperature, which is due to its partial melting. Fluorapatite remained present and it was identified only in the M2 XRD trace, in which phosphate was added. New crystalline phases namely anorthite, akermanite, diopside, cristobalite, hematite and magnetite, were formed in both sintered samples. Anorthite formation results from the reaction between free CaO released upon decarbonation, with alumino-silicates from dehydroxylation of clay minerals **(Liao et al 2011; Loutou, 2013)**. Hence, this newly crystalline phase was more abundant in the M2 sample, which is richer in calcium carbonate

https://doi.org/10.1180/clm.2024.10 Published online by Cambridge University Press

than the M1 sample. Tthe intensity of the anorthite peaks was strongest in the M2 fired at 1100°C and 1125°C but the peak intensities decreased slightly at 1150°C, probably due to partial melting. Akermanite and diopside were identified in both samples after firing at 1150°C. They resulted from the reaction between Ca, Mg and the Al and Si released from the decomposition of clayey materials upon firing. The peak intensities were slightly larger in the M2 LWA than that in the M1 LWA. This can be explained by the contribution of magnesium oxide (MgO) resulting from the decomposition of dolomite present in additives. Cristobalite peak intensities (4.05 Å and 2.51Å) are observed in all the pellets and it is more pronounced in the M1 pellet fired at 1150°C. The peak intensities of newly formed cristobalite slightly increased with increasing temperature from 1100 to 1150°C, while the quartz reflection intensities decreased. Such mineralogical changes suggest that some cristobalite might have been derived from the transformation of quartz with increasing firing temperatures. Indeed, quartz first begins to melt at 1100°C and part of the molten quartz is transformed into cristobalite. These results are consistent with previous studies **(Aras et al., 2019),** which reported that cristobalite is mainly formed from SiO_2 released by decomposition of clay minerals at ~ 1100°C and from the transformation of quartz with rising firing temperatures up to 1200°C, as this is demonstrated by the gradual decrease in quartz peak intensities and the gradual increase in cristobalite peak intensities. Hematite was recorded in the all XRD traces from 1100°C and its reflection intensities increased with increasing temperature. The hematite in M1 sample formed from oxidation of Fe that was initially present in the crystal lattice of clay minerals (i.e Fe-smectite) after structural decomposition. The M2 XRD traces contain magnetite. The dark red color of the M1 LWA might be attributed to hematite enrichment. However the M1 LWA shows a slightly dark color in comparison to M2 LWA, which can be related to the magnetite formation after transformation probably of hematite. Magnetite might result from the reduction of hematite in the presence of carbonates (Ayati et al., 2018; Pei et al., 2022).

Morphology and microstructure of the lightweight aggregates

Figure 6 shows the effects of the sintering temperature on the characteristics of LWAs based on SmC. The expansion gradually enhanced with the increase of sintering temperature from 1100°C to 1150°C (Fig. 6). Both M1 and M2 formulations show maximum expansion at 1150°C (Fig. 6). Some trials conducted at higher temperatures (not shown) showed excessive melting and deformation, hence 1150°C can be considered as the optimal firing temperature.

https://doi.org/10.1180/clm.2024.10 Published online by Cambridge University Press

Fired pellets show stable shape and noticeable bloating. An internal porous structure was developed, but some samples show unvitrified surface with pores and cracks (Fig. 6). The M1 pellets are more prone to such defects. These cracks were probably caused by excessive pressure of gases entrapped in the inner pores. **Fakhfakh et al. (2007)** also reported cracks formation in the external surface of lightweight aggregates produced from smectite clay and sintered in the same temperature range. These authors suggest this is a common problem when plastic clays are used, due to the excessive shrinkage upon firing. This is particularly critical when, an expressive amount of gas released from carbonates decomposition almost simultaneously **(Liu et al., 2017)**. The desirable bloating is favored but there are risks of crack formation (Fig. 6). The addition of phosphate sludge and palygorskite rich-sediment minimized that problem. The morphology of such samples shows a vitrified outer surface, denoting better fluxing characteristics of the M2 mix (Fig. 6). This assures higher deformation and capacity to contain the formed gas without crack formation. In any case, some single pin-holes are visible to the naked eye (Fig. 6).

The SEM images of the LWAs produced from M1 (100% SmC) and M2 (50% SmC, 25% PhS and 25% PalS) formulations and sintered at 1100, 1125 and 1150°C are shown in Figure 7. For both M1 and M2 LWAs fired at 1100°C, the SEM micrographs showed a low porosity characterized by some small and closed pores, scattered in a liquid-rich environment which took place during the sintering process and in which unreacted particles are visible, due to lack of sufficient sintering. At 1125 °C, the SEM images of the M1 sample without addition were noticeably different from those of the M2 sample containing phosphate sludge and palygorskite. The M1 LWA is characterized by a weak porous structure, predominantly with a large number of small pores with few oval-shaped and sometimes elongated large pores. The development of few large pores ranging in size from 500 μm to 3 mm is clearly observed in the inner core; however, the shell part shows a dense microstructure containing some macropores 100 μm to 350 μm in size and abundant small pores 20 μm to 100 μm in size, opposite to the core part.

Unlike the M1 LWA, the M2 LWA is characterized by a compact structure. The addition of PhS and Pal enhanced formation of molten phases. Therefore, with continuous heating at 1125°C, the unreacted solid phases observed at 1100°C began to dissolve, yielding a molten phase that covers the remaining particles. The liquid phase filled the voids around the remaining particles and created a dense microstructure.

https://doi.org/10.1180/clm.2024.10 Published online by Cambridge University Press

The SEM images of M1 and M2 fired at 1150°C, revealed the development of a high porous network for both samples particularly for M2 with additives. For both pellets, a relatively dense shell covering the internal core was developed (Fig. 7). The outer shell was much less porous than the interior core.

The developed porous structure involves a large proportion of macropores with size between 200 μm and 700 μm in the shell and between 200 μm and 3mm in the inner core particularly for M2 sample. The pore size distribution is inhomogeneous, since much smaller pores are also present. The development of large pores is mainly governed by the internal pressure of the trapped gas during sintering **(González et al., 2010)**.

Most of the pores are not interconnected and few interior pores are well-interconnected or separated by a thin wall particularly for M2 pellets (Fig. 7). These enclosed pores are observed inside the large spherical or ovoid pores in the inner core or close to the surface of LWAs. However the pores of the shell are more isolated and the walls between the pores are thicker.

The development of pores in M1 LWA is due to thermal expansion of SmC clay at high temperature, while in M2, gases liberated from the decomposition of PhS and Pal, can create internal pressure to increase the volume of the pores initially developed at 1125°C. At this stage, the released gas may be more easily trapped by the liquid phase and bloating is more noticeable.

This microstructure has a great effect on water absorption. Pores structure with a large number of connected pores in the LWAs might provide spaces to accommodate water and improve water absorption. However a pore structure containing only non-connected or enclosed pores leads to low water absorption **(Moreno-Maroto et al., 2017)**.

Figure 8 displays the EDS analysis results for randomly selected points on the surface and core of both M1 and M2 at different sintering temperatures. Chemical elemental analysis of the LWAs using EDS reveal the presence of Si, Al, Fe, Na, K, and O, elements resulting from the decomposition of the raw minerals present in the clayey materials, especially the SmC and Pal samples. Therefore, sintering reactions formed new crystalline phases in agreement with the XRD results, which show the Si-rich, Al-rich and K, Ca-Na-rich mineral phases, composing the LWAs matrix as it was confirmed by EDS mapping (Fig. 9a, 9b). The elemental composition of M2 LWA has changed due to the composition of the additives with an enrichment in particular of Ca, P and S, F and minor Cl, which derive from the decomposition

https://doi.org/10.1180/clm.2024.10 Published online by Cambridge University Press

of carbonate-fluorapatite and gypsum present in the phosphate sludge. The presence of iron in both M1 and M2 formulations is related to the starting raw materials composition, whereby the sintering at high temperatures promotes the formation of ferrous oxides like hematite detected by XRD. Additionally, EDS mapping of M2 (Fig. 9b) clearly shows Ca, P-rich sectors homogeneously distributed in the LWA matrix. However, S, F and Cl show a heterogeneous distribution and their concentration is probably too low to show clear variations. Non-volatile potentially hazardous species tend to be immobilized/become inert in the matrix due to firing (Wei, 2015; Franus et al., 2016). This behavior is common in the formulation of ceramics.

LWAs properties characterization

The results of the expansion properties of the pellets fired at different temperatures including bloating index, bulk density, water absorption, and compressive strength as a function of the firing temperature are shown in Table 5 and Figure 10. The values obtained for each property are the average of 6 measurements obtained from each aggregate variety. The bloating index (BI) increases with firing temperature, more gradually with M1 pellets (Table 5, Fig. 10). The BI of these samples reached 20% at 1150°C, demonstrating the expansive behavior of the used smectite clay (SmC). On M2 samples the increase of BI with temperature is not linear and a sharp increase was registered from 1125 to 1150°C. At this temperature, the expansion is almost double that of M1 samples. Bloating is a complex phenomenon that causes volume increase upon firing, due to gas release (CO_2, CO, O_2, SO_3) from certain components (organic matter, carbonates, Fe_2O_3, etc). The gasses are trapped by the fairly viscous liquid phase and generate inner porosity **(González-Corrochano et al., 2010, 2011; Dondi et al., 2016, Moreno-Maroto et al., 2020, Molinari et al., 2020)**. The pressure of trapped gases increases with temperature, causing bloating or expansion **(González-Corrochano et al., 2010)**. Palygorskite rich-sediment and phosphate sludge promote gas formation, due to their relative high content of carbonaceous compounds. This effect is more evident on PhS, while PalS accelerates the formation of fluxing phases, that is crucial to avoid gas release to the exterior of the samples. **Wang et al. (2022)**, studied the influence of palygorskite in the firing process of clay mixtures, confirming its fluxing characteristics.

The bulk density of pellets is inversely proportional to the bloating index, whereby it decreases as the firing temperature increases from 1100 to 1150°C. The bulk density of the both LWAs slightly decreased when the firing temperature increased from 1000°C to 1125°C, although significant bloating was not recorded at this temperature range. When the temperature increased

https://doi.org/10.1180/clm.2024.10 Published online by Cambridge University Press

to 1150°C, pellets showed excessive bloating which resulted to an important decrease in bulk density. Bloating is associated to pore formation that decreases sample weight. The M2 pellets tend to be lighter than the M1 ones at the same firing temperature, and progress with this variable is also similar (but inverse) to the one discussed for the BI. The lowest values of bulk density 0.6 g/cm^3 and 0.8 g/cm^3, were obtained by firing at 1150°C and it is well clear that the bulk density of M2 was lower than that of M1. According to European standard EN-13055-1, a good quality LWA must show density < 1.2 g/cm^3. **Dondi et al. (2016)**, on a systematic review of LWAs, established the following classification according to the density: group I: very low density = 0.3-0.6 g/cm^3; group II: low density = 0.61-0.99 g/cm^3; group III: medium density = 1.0-1.4 g/cm^3 and group IV: high density = >1.4 g/cm^3. SmC pellets (M1) sintered at 1150°C belong to group II (0.8 g/cm^3), while M2 pellets fired at the same temperature belong to group I (0.6 g/cm^3). Most results are fully consistent with the literature, where the effects of temperature and composition on bloating of LWAs are detailed **(Soltan et al., 2016; Liu et al., 2017, 2018; Yun Cao et al., 2019; Moreno-Maroto et al., 2020; Li et al., 2021; Sossio Fabio Graziano et al., 2022)**.

The water absorption (WA) of pellets (Table 5, Fig. 10), may be used to estimate the formation of vitreous phase and abundance of open pores. As more pores are formed upon heating there will be tendency for an increase of WA, unless abundant vitreous phases form to seal the pores and to create an impermeable shell. In the M1 pellets the incipient fluxing character of the SmC clay does not generate enough vitreous phases, so the WA tends to increase with increasing firing temperature. In the M2 samples that increment is only visible at 1150°C, due to the fast formation of porosity. In any case, the WA values are not very high, indicating that a significant fraction of closed pores was formed and rendering the LWAs less accessible to water.

The compressive strength of pellets is expected to show an inverse relationship with WA and density, because porous samples tend to be mechanically weaker. In general, these trends were observed in this study (Table 5, Fig. 10). In the M1 pellets the change of firing temperature causes a gradual variation in the compressive strength (similar to the remaining properties), while in M2 samples change occurs fast in the range 1125-1150°C. With addition of PhS and PalS, the compressive strength increased largely while the density did not increase significantly. The formation of a high amount of a vitreous phase, which fills pores might be responsible for the higher strength of the M2 aggregates. However, with increasing temperature, the strength of the LWAs would inevitably decrease, because the developed large pores would render the LWAs significantly weak. Despite the lower density of these M2 pellets in comparison to their

https://doi.org/10.1180/clm.2024.10 Published online by Cambridge University Press

M1 counterparts, the compressive strength of the former is higher due to the extended formation of vitreous phases. Addition of PalS and PhS to the SmC clay seems to assure a better balance of properties, namely lower density but higher mechanical strength. These properties are comparable to those of light commercial expanded aggregates (ECA) (Table 5), suggesting the possibility of producing LWAs from phosphate waste and palygorskite-rich sediments.

CONCLUSION

In this work, laboratory prepared pellets based on a smectite clay (SmC) and formulated with addition of palygorskite rich-sediment (PalS) and phosphate sludge (PhS) (25 wt% each) expand when fired at 1100-1150°C. The expansive potential of the tested formulations (M1 and M2, respectively) allows their use in the fabrication of LWAs. The optimal firing temperature was 1150°C, assuring maximum expansion of both formulations. Fired pellets showed minimum density (0.8 and 0.6 g/cm^3 for M1 and M2, respectively), while the compressive strength is adequate to assure their integrity in further formulations.

In the pure SmC pellets the evolution of studied properties (density, compressive strength, water absorption) with increasing firing temperature is gradual and monotonous. The addition of PalS and PhS changed that pattern, with slower progress between 1100 and 1125°C and then a sudden change at 1150°C. This results from the stronger fluxing characteristics of the PalS above the intermediate tested temperature, while PhS enhances gas formation simultaneously with the development of an adequately viscous liquid phase to trap the gases released. This would cause considerable expansion with a developed internal porous structure. Total porosity, pore connectivity, and pore size distribution define the pore structure of the LWAs, and consequently they affect its bulk density, water absorption, and compressive strength. The addition of PalS and PhS seems to assure a better balance of LWA properties, namely lower density and a greater mechanical strength. The recycling of such waste/by-products has an obvious environmental impact, contributing to the circular economy. The, S, F and Cl occur in very low concentration in the LWA matrix, to cause environmental issues. However, emission of gases after decomposition of PhS requires precautions at the industrial scale.

The production of LWA from clay and the used additives, can be industrially feasible, on the condition that the manufacturing process, specifically the expansion phenomenon, is controlled to produce LWA with a good porous structure and low density.

ACKNOWLEDGEMENTS

https://doi.org/10.1180/clm.2024.10 Published online by Cambridge University Press

This work was carried out as part of a research internship in the Department of Materials and Ceramic Engineering, University of Aveiro Portugal, with the support of the scientific and technological research program of the University of Gabes, Tunisia. The acknowledgement is addressed to Pr. João Labrincha, for availability, assistance and for valuable comments to do this work well.

Declarations

Conflict of Interest The authors declare that they have no conflict of interest.

https://doi.org/10.1180/clm.2024.10 Published online by Cambridge University Press

REFERENCES

- De Jesus Fernandes Pinto, S. (2005). Valorização de resíduos da indústria da celulose na produção de agregados leves, PhD Thesis. Univ. Aveiro, Aveiro, Portugal, 118 pp.
- Murray, H.H. (2000). Traditional and new applications for kaolin smectite, and palygorskite: a general overview. *Applied Clay Science,* **17**, 207–221.
- Wei, N. (2015). Leachability of heavy metals from lightweight aggregates made with sewage sludge and municipal solid waste incineration fly ash. *International Journal of Environmental Research and Public Health*, **12(5)**, 4992-5005.
- Anan, T. I., & Abd El-Wahed, A. G. (2017). The Maastrichtian-Danian Dakhla Formation, Eastern Desert, Egypt: Utilization in manufacturing lightweight aggregates. *Applied Clay Science,* **150**, 10–15.
- Frost, R.L., & Ding, Z. (2003). Controlled rate thermal analysis and differential scanning calorimetry of sepiolites and palygorskites, *Thermochimica Acta,* **397(1–2)**, 119–128.
- Liao, Y., & Huang, C. (2011). Effects of heat treatment on the physical properties of lightweight aggregate from water reservoir sediment. *Ceramics International,* **37(8)**, 3723–3730.
- Saadaoui, I., & Eloussaief, M. (2017). Analytical Characterization of Eocene Deposits for the Identification of Dolomitic-Palygorskite in Jebel Rheouis, Central Tunisia. In Euro-Mediterranean Conference for Environmental Integration. Springer, Cham. 1165–1167.
- Suárez, M., & García-Romero, E. (2011). Advances in the crystal chemistry of sepiolite and palygorskite. *In Developments in clay science*, **3**, 33-65.
- Trabelsi, W., & Tlili, A. (2017). Phosphoric acid purification through different raw and activated clay materials (Southern Tunisia), *Journal of African Earth Sciences,* **129**, 647–658.
- Volland, S., & Brötz, J. (2015). Lightweight aggregates produced from sand sludge and zeolitic rocks. *Construction and Building Materials,* **85**, 22–29.
- Wang, W., & Wang, A. (2016). Recent progress in dispersion of palygorskite crystal bundles for nanocomposites. *Applied Clay Science,* **119**-*1*, 18–30.
- Abbaslou, H., Ghanizadeh, A.R., & Amlashi, A.T. (2016). The compatibility of bentonite/sepiolite plastic concrete cut-off wall material. *Construction and Building Materials*, **124,** 1165–1173.

https://doi.org/10.1180/clm.2024.10 Published online by Cambridge University Press

- Arab, P. B., Araújo, T. P., & Pejon, O. J. (2015). Identification of clay minerals in mixtures subjected to differential thermal and thermogravimetry analyses and methylene blue adsorption tests. *Applied Clay Science,* **114**, 133–140.
- Da Silva, M. L., Batezelli, A., & B. Ladeira, F. S. (2018). Genesis and paleoclimatic significance of palygorskite in the cretaceous paleosols of the Bauru Basin, Brazil. *Catena,* **168**, 110–128.
- Franus, M., Barnat-Hunek, D., & Wdowin, M. (2016). Utilization of sewage sludge in the manufacture of lightweight aggregate. *Environmental monitoring and assessment*, 188, 1-13.
- Frayyeh, Q.J., Abbas, W. A., & Hussein, M. J. (2014). Producing Lightweight Concrete Aggregate from Iraqi Attapulgite. Conference: Sustainable Solutions in Structural Engineering and Construction, 2nd. Australasia and South East Asia Conference At: Bangkok, Thailand: ISBN: 978-0-996437-0-0.
- Tlili, A., Felhi, M., & Montacer, M. (2010). Origin and depositional environment of palygorskite and sepiolite from the Ypresian phosphatic series, Southwestern Tunisia. *Clays and Clay Minerals,* **58(4)**, 573–584.
- Zhao, D., Zhou, J., & Liu, N. (2006). Preparation and characterization of Mingguang palygorskite supported with silver and copper for antibacterial behavior, *Applied Clay Science,* **33(3–4)**, 161–170.
- Abdelfattah, M.M., Géber, R., Abdel-Kader, N.A., & Kocserha, I. (2022). Assessment of the mineral phase and properties of clay-Ca bentonite lightweight aggregates. *Arabian Journal of Geosciences,* **15(2)**, 1–14.
- Franus, M., Panek, R., Madej, J., & Franus, W. (2019). The properties of fly ash derived lightweight aggregates obtained using microwave radiation, *Construction and Building Materials,* **227**, 116677.
- Liu, M., Wang, C., Bai, Y., & Xu, G. (2018). Effects of sintering temperature on the characteristics of lightweight aggregate made from sewage sludge and river sediment. *Journal of Alloys and Compounds,* **748**, 522–527.
- Liu, P., Farzana, R., Rajaro, R., & Sahajwalla, V. (2017). Lightweight expanded aggregates from the mixture of waste automotive plastics and clay. *Construction and Building Materials,* **145**, 283–291.
- Mahmoudi, S., Bennour, A., Srasra, E., & Zargouni, F. (2017). Characterization, firing behavior and ceramic application of clays from the Gabes region in South Tunisia. *Applied Clay Science,* **135**, 215–225.

https://doi.org/10.1180/clm.2024.10 Published online by Cambridge University Press

- Pei, J., Pan, X., Qi, Y., & Yu, H. (2022). Ganfeng Tu, Preparation and characterization of ultra-lightweight ceramsite using non-expanded clay and waste sawdust. *Construction and Building Materials,* **346**, 128410.
- Abdelmalek, B., Rekia, B., Youcef, B., Lakhdar, B., & Nathalie, F. (2017). Mineralogical characterization of Neogene clay areas from the Jijel basin for ceramic purposes (NE Algeria -Africa). *Applied Clay Science*, **136***,* 176–183.
- Allouche, F., Eloussaief, M., Ghrab, S., & Kallel, N. (2020). Clay material of an Eocene deposit (Khanguet Rheouis, Tunisia) : Identification using geochemical and mineralogical characterization. *Clays and Clay Minerals,* **68**, 262–272.
- Alvarez, A., Santaren, J., Esteban-Cubillo, A., & Aparicio, P. (2011). Current industrial applications of palygorskite and sepiolite. In Developments in clay science, **3**, 281-298.
- Ayati, B., Ferrándiz-Mas, V., Newport, D., & Cheeseman, C. (2018). Use of clay in the manufacture of lightweight aggregate. *Construction and Building Materials,* **162**, 124-131.
- Chalouati, Y., Bennour, A., Mannai, F., & Srasra, E. (2020). Characterization, thermal behaviour and firing properties of clay materials from Cap Bon Basin, north-East Tunisia, for ceramic applications. *Clay Minerals,* **55(4)**, 351–365.
- Karunadasa, K. S.P., Manoratne, C.H., Pitawala, H.M.T.G.A., & Rajapakse, R.M.G. (2019). Thermal decomposition of calcium carbonate (calcite polymorph) as examined by in-situ high-temperature X-ray powder diffraction. *Journal of Physics and Chemistry of Solids,* **134**, 21–28.
- Martínez, J. D., Betancourt-Parra, S., Carvajal-Marín, I., & Betancur-Vélez, Mariluz. (2018). Ceramic light-weight aggregates production from petrochemical waste and carbonates ($NaHCO_3$ and $CaCO_3$) as expansion agents. *Construction and Building Materials,* **180**, 124–133.
- Molinari, C., Zanelli, C., Guarini, G., & Dondi, M. (2020). Bloating mechanism in lightweight aggregates: Effect of processing variables and properties of the vitreous phase. *Construction and Building Materials,* **261***,* 119980.
- Alabarse, F. G., Conceição, R. V., Balzaretti, N. M., Schenato, F., & Xavier, A. M. (2011). In-situ FTIR analyses of bentonite under high-pressure. *Applied Clay Science,* **51 (1–2)**, 202–208.
- Chen, P., Zhong, H., Li, X., Li, M., & Zhou, S. (2021). Palygorskite@Co_3O_4 nanocomposites as efficient peroxidase mimics for colorimetric detection of H_2O_2 and ascorbic acid. *Applied Clay Science,* **209**, 106109.

https://doi.org/10.1180/clm.2024.10 Published online by Cambridge University Press

- Dabbebi, R., Barroso de Aguiar, J.L., Camões, A., Samet, B., & Baklouti, S. (2018). Effect of the calcinations temperatures of phosphate washing waste on the structural and mechanical properties of geopolymeric mortar. *Construction and Building Materials,* **185**, 489–498.
- Daoudi, L., Knidiri, A., El Boudour El Idrissi, H., Rhouta, B., & Fagel, N. (2015). Role of the texture of fibrous clay minerals in the plasticity behavior of host materials (Plateau du Kik, Western High Atlas, Morocco). *Applied Clay Science,* **118**, 283–289.
- Ding, C., Sun, T., Shui, Z., Xie, Y., & Ye, Z. (2022). Physical properties, strength, and impurities stability of phosphogypsum-based cold-bonded aggregates. *Construction and Building Materials,* **331**, 127307.
- González-Corrochano, B., Alonso-Azcárate, J., Rodas, F.J., Luque, M., & Barrenechea, J.F. (2010). Microstructure and mineralogy of lightweight aggregates produced from washing aggregate sludge, fly ash and used motor oil. *Cement and Concrete Composites,* **32**, 694–707.
- González-Corrochano, B., Alonso-Azcárate, J., Rodas, F.J., Barrenechea, J.F., & Luque, M. (2011). Microstructure and mineralogy of lightweight aggregates manufactured from mining and industrial wastes. *Construction and Building Materials,* **25**, 3591–3602.
- Loutou, M., Hajjaji, M., Mansori, M., Favotto, C., & Hakkou, R. (2013). Phosphate sludge: Thermal transformation and use as lightweight aggregate material. *Journal of Environmental Management,* **130**, 354-360.
- Loutou, M., Taha, Y., Benzaazoua, M., Daafi, Y., & Hakkou, R. (2019). Valorization of clay by-product from moroccan phosphate mines for the production of fired bricks, *Journal of Cleaner Production,* **229**, 169-179.
- Moreno-Maroto, J.M., González-Corrochano, B., Alonso-Azcárate, J., Rodríguez, L., & Acosta, A. (2017). Manufacturing of lightweight aggregates with carbon fiber and mineral wastes. *Cement and Concrete Composites,* **83***,* 335–348.
- Wang, S., Gainey, L., Wang, X., Mackinnon, Ian D.R., & Xi, Y. (2022). Influence of palygorskite on in-situ thermal behaviours of clay mixtures and properties of fired bricks. *Applied Clay Science,* **216**, 106384.
- Boussen, S., Sghaier, D., Chaabani, F., Jamoussi, B., Ben Messaoud, S., & Bennour, A. (2015). The rheological, mineralogical and chemical characteristic of the original and the Na_2CO_3-activated Tunisian swelling clay (Aleg Formation) and their utilization as drilling mud. *Applied Clay Science,* **118***, 344*–353.

https://doi.org/10.1180/clm.2024.10 Published online by Cambridge University Press

- Cao, Y., Liu, R., Xu, Y., Ye, F., Xu, R., & Han, Y. (2019). Effect of SiO_2, Al_2O_3 and CaO on characteristics of lightweight aggregates produced from MSWI bottom ash sludge (MSWI-BAS). *Construction and Building Materials,* **205**, 368–376.
- Fontaine, F., Christidis, G.E., Yans, J., Hollanders, S., Hoffman, A., & Fagel, N. (2020). Characterization and origin of two Fe-rich bentonites from Westerwald (Germany). *Applied Clay Science,* **187**, 105444.
- Lakbita, O., Rhouta, B., Maury, F., Senocq, F., Amjoud, M., & Daoudi, L. (2019). On the key role of the surface of palygorskite nanofibers in the stabilization of hexagonal metastable β-Ag_2CO_3 phase in palygorskite-based nanocomposites. *Applied Clay Science,* **172***,* 123–134.
- Liu, Y., Wan, W., Yang, F., Hu, C., Liu, Z., & Wang, F. (2022). Performance of glass-ceramic-based lightweight aggregates manufactured from waste glass and muck. *Ceramics International,* **48**, 23468-23480.
- Mabroum, S., Aboulayt, A., Taha, Y., Benzaazoua, M., Semlal, N., & Hakkou, R. (2020). Elaboration of geopolymers based on clays by-products from phosphate mines for construction applications. *Journal of Cleaner Production,* **261**, 121317.
- Mañosa, J., Formosa, J., Giro-Paloma, J., Maldonado-Alameda, A., Quina, M.J., & Chimenos, J.M. (2021). Valorisation of water treatment sludge for lightweight aggregate production. *Construction and Building Materials,* **269**, 121335.
- Moreno-Maroto J.M., Uceda-Rodríguez, M., Cobo-Ceacero, C.J., Cotes-Palomino, T., Martínez-García, C., & Alonso-Azcárate, J. (2020). Studying the feasibility of a selection of Southern European ceramic clays for the production of lightweight aggregates. *Construction and Building Materials,* **237**, 117583.
- Moukannaa, S., Nazari, A., Bagheri, A., Loutou, M., Sanjayan, J.G., & Hakkou, R. (2019). Alkaline fused phosphate mine tailings for geopolymer mortar synthesis: Thermal stability, mechanical and microstructural properties. *Journal of Non-Crystalline Solids, 511*, 76–85.
- Soltan, A. M. M., Kahl, W.A., Abd EL-Raoof, F., El-Kaliouby, B. A. H., Serry, N. A., & Abdel-Kader, M. A.K. (2016). Lightweight aggregates from mixtures of granite wastes with clay. *Journal of Cleaner Production,* **117**, 139–149.
- Wang, S., Gainey, L., Baxter, D., Wang, X., Mackinnon, Ian D.R., & Xi, Y. (2021). Thermal behaviours of clay mixtures during brick firing: A combined study of in-situ XRD, TGA and thermal dilatometry. *Construction and Building Materials,* **299**, 124319.

https://doi.org/10.1180/clm.2024.10 Published online by Cambridge University Press

- Yang, L., Ma, X., Hu, X., Liu, J., Wu, Z., & Shi, C. (2022). Production of lightweight aggregates from bauxite tailings for the internal curing of high-strength mortars. *Construction and Building Materials,* **341**, 127800.
- Zhang, Y., Wang, L., Wang, F., Sun, J., Tang, Q., & Liang, J. (2019). Effects of palygorskite on physical properties and mechanical performances of bone china. *Applied Clay Science,* **168**, 287–294.
- Bayoussef, A., Loutou, M., Taha, Y., Mansori, M., Benzaazoua, M., Manoun, B., & Hakkou, R. (2021a). Use of clays by-products from phosphate mines for the manufacture of sustainable lightweight aggregates. *Journal of Cleaner Production*, **280-1**, 124361.
- Bayoussef, A., Oubani, M., Loutou, M., Taha, Y., Benzaazoua, M., Manoun, B., & Hakkou, R. (2021b). Manufacturing of high-performance ceramics using clays by-product from phosphate mines. *Materials Today: Proceedings,* **37(3)**, 3994–4000.
- Ettoumi, M., Jouini, M., Neculita, C.M., Bouhlel, S., Coudert, L., Haouech, I., & Benzaazoua, M. (2020). Characterization of Kef Shfeir phosphate sludge (Gafsa, Tunisia) and optimization of its dewatering. *Journal of Environmental Management,* **254**, 109801.
- Fan, Z., Zhou, S., Xue, A., Li, M., Zhang, Y., Zhao, Y., & Xing, W. (2021). Preparation and properties of a low-cost porous ceramic support from low-grade palygorskite clay and silicon-carbide with vanadium pentoxide additives. *Chinese Journal of Chemical Engineering,* **29**, 417–425.
- Zhang, Y., Yu, C., Hu, P., Tong, W., Lv, F., Chu, P. K., & Wang, H. (2016). Mechanical and thermal properties of palygorskite poly(butylene succinate) nanocomposite. *Applied Clay Science,* **119**, 96–102.
- De Souza, C., De Jesus, T., Dos Santos, R., Bomfim, L., Bertolino, L., De Andrade, D., D´Avila, L.A., & Spinelli, L. (2021). Characterization of Brazilian palygorskite (Guadalupe region) and adsorptive behaviour for solvatochromic dyes. *Clay Minerals,* **56-1**, 55–64.
- Dondi, M., Cappelletti, P., D'Amore, M., de Gennaro, R., Graziano, S.F., Langella, A., Raimondo, M., & Zanelli, C. (2016). Lightweight aggregates from waste materials: Reappraisal of expansion behavior and prediction schemes for bloating. *Construction and Building Materials,* **127**, 394–409.
- Ettoumi, M., Jouini, M., Neculita, C.M., Bouhlel, S., Coudert, L., Haouech, I., Taha, Y., & Benzaazoua, M. (2021). Characterization of phosphate processing sludge from Tunisian mining basin and its potential valorization in fired bricks making. *Journal of Cleaner Production,* **284**, 124750.

https://doi.org/10.1180/clm.2024.10 Published online by Cambridge University Press

- Ezzatahmadi, N., Millar, G. J., Ayoko, G.A., Zhu, J., Zhu, R., Liang, X., He, H., & Xi, Y. (2019). Degradation of 2,4-dichlorophenol using palygorskite-supported bimetallic Fe/Ni nanocomposite as a heterogeneous catalyst. *Applied Clay Science,* **168**, 276–286.
- Graziano, S. F., Zanelli, C., Molinari, C., de Gennaro, B., Giovinco, G., Correggia, C., Cappelletti, P., & Dondi, M. (2022). Use of screen glass and polishing sludge in waste-based expanded aggregates for resource-saving lightweight concrete. *Journal of Cleaner Production,* **332**, 130089.
- Harech, M. A., Mesnaoui, M., Abouliatim, Y., Elhafiane, Y., Benhammou, A., Abourriche, A., Smith, A., & Nibou, L. (2021). Effect of temperature and clay addition on the thermal behavior of phosphate sludge. *Boletín de la Sociedad Española Cerámica y Vidrio,* **60(3)**, 194-204.
- Harech, R., Dabbebi, M. A., Abouliatim, Y., Elhafiane, Y., Smith, A., Mesnaoui, M., Niboue, L., & Baklouti, S. (2022). A comparative study of the thermal behaviour of phosphate washing sludge from Tunisia and Morocco. *Journal of Thermal Analysis and Calorimetry,* **147**, 5677–5686.
- Li, X., He, C., Lv, Y., Jian, S., Jiang, W., Jiang, D., Wu, K., & Dan, J. (2021). Effect of sintering temperature and dwelling time on the characteristics of lightweight aggregate produced from sewage sludge and waste glass powder. *Ceramics International,* **47-23**, 33435–33443.
- Wei, D., Zhou, S., Li, M., Xue, A., Zhang, Y., Zhao, Y., Zhong, J., & Yang, D. (2019). PVDF/palygorskite composite ultrafiltration membranes: Effects of nano-clay particles on membrane structure and properties. *Applied Clay Science,* **181**, 105171.
- Fakhfakh, E., Hajjaji, W., Medhioub, M., Rocha, F., Galindo, A.L., Setti, M., Kooli, F., Zargouni, F., & Jamoussi, F. (2007). Effect of sand addition on production of lightweight aggregates from Tunisian smectite-rich clayey rocks. *Applied Clay Science,* **35**, 228–237.
- Sun, Y., Li, J., Chen, Z., Xue, Q., Sun, Q., Zhou, Y., Chen, X., Liu, L., & Sun Poon, C. (2021). Production of lightweight aggregate ceramsite from red mud and municipal solid waste incineration bottom ash : Mechanism and optimization. *Construction and Building Materials,* **287**, 122993.
- EN-1097-6 (2013). Tests for mechanical and physical properties of aggregates. Part 6: Determination of particle density and water absorption. European Committee for Standardization.

https://doi.org/10.1180/clm.2024.10 Published online by Cambridge University Press

Table 1. Composition of the tested formulations (wt%).

Composition Mixture	Smectite Clay	Palygorskite rich-sediment	Phosphate sludge
M1	100	0	0
M2	50	25	25

Table 2. Chemical composition (wt %) of the studied materials and other clays mentioned in the literature that were used in the LWAs production.

Sample	LOI	CaO	MgO	SiO_2	Fe_2O_3	Al_2O_3	Na_2O	K_2O	SO_3	P_2O_5	F
SmC	16.8	2.24	2.23	51.6	6.67	13.3	2.35	0.85	3.9	-	-
PalS	15.8	22.0	3.39	34.1	4.03	8.94	0.57	1.56	8.43	0.11	0.14
PhS	15.6	31.3	2.01	21.9	1.51	3.8	0.79	0.92	3.73	16.7	1.34
Technological sample (Anan et al., 2017)	14.70	1.32	2.34	50.87	3.69	22.12	1.88	1.02	0.60	0.12	-
Clay (Liu et al., 2017)	-	0.45	1.27	58.02	7.13	19.81	0.80	2.53	-	0.20	-
PY2 (Moreno-Maroto et al, 2020)	6.7	2.0	2.5	64.4	5.5	14.0	0.4	3.2	-	-	-

https://doi.org/10.1180/clm.2024.10 Published online by Cambridge University Press

Table 3. Mineralogical composition of the starting raw materials. Sme, Smectite; Plg, palygorskite, Qz, quartz; Cal, calcite; Dol, dolomite; Gp, gypsum; Fap, fluoroapatite. + = 1-5%; ++ = 6-25%; +++ = 26-50%; ++++ =51-75%; +++++ = 76-100%

Sample Composition (%)	Sme	Plg	Qz	Cal	Dol	Gp	Fap
SmC	+++++		++	+	-	+	-
PalS		+++	++	+++	+	++	-
PhS	+		+	++	+	+	+++

Table 4. Particle size distribution and Atterberg limits (%) of the raw materials.

Sample	<2 µm	2–63 µm	>63 µm	Liquid limit (Ll)	Plastic limit (Pl)	Plasticity index (PI)
SmC	40	60	0	64	32	32
PalS	8	92	0	52	13	39
PhS	10	42	48	-	-	-

https://doi.org/10.1180/clm.2024.10 Published online by Cambridge University Press

Table 5. Physical properties of the studied LWAs and the commercial LWA: Expanded Clay Aggregate - ECA.

Temperature of sintering (°C) **Composition**		**1100**	**1125**	**1150**
M1	Bloating Index (%)	11.5	15.7	29.8
	Particle Density (g/cm^3)	1.33	1.05	0.8
	Water Absorption after 24 h (wt %)	5	7	10
	Compressive Strength (MPa)	2.77	1.535	0.67
	Expansion	Low	Good	Very good
M2	Bloating Index (%)	5.1	6.2	38.5
	Particle Density (g/cm^3)	1.05	1.02	0.6
	Water Absorption after 24 h (wt %)	6	4	12
	Compressive Strength (MPa)	3.34	3.83	0.86
	Expansion	Low	Good	The best
Expanded Clay Aggregate - ECA	Particle Density (g/cm^3)	0.24 to 0.88		
	Water Absorption (wt%)	18-23		
	Compressive Strength (MPa)	0.6 to 3		

https://doi.org/10.1180/clm.2024.10 Published online by Cambridge University Press

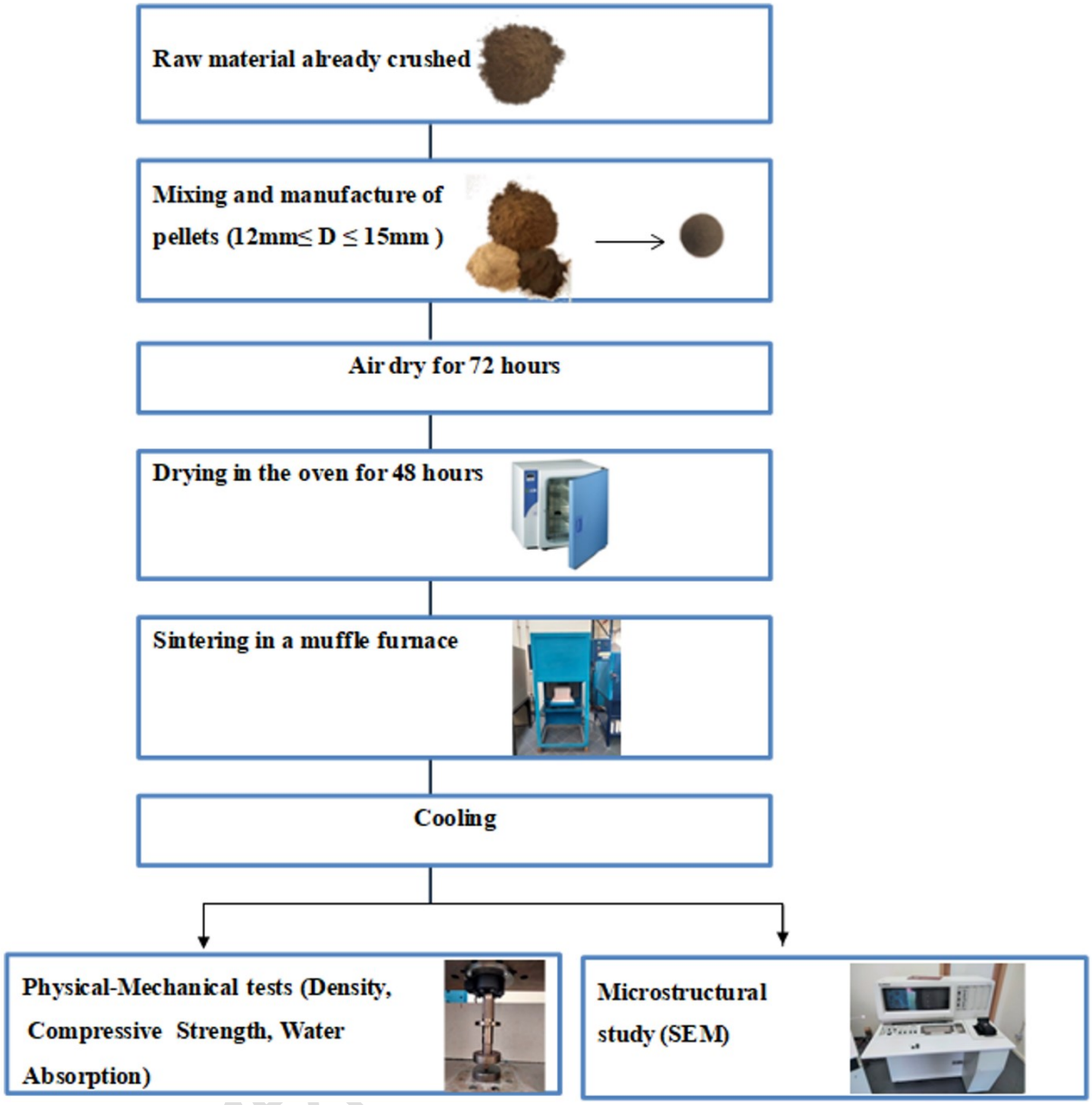

Figure 1.

https://doi.org/10.1180/clm.2024.10 Published online by Cambridge University Press

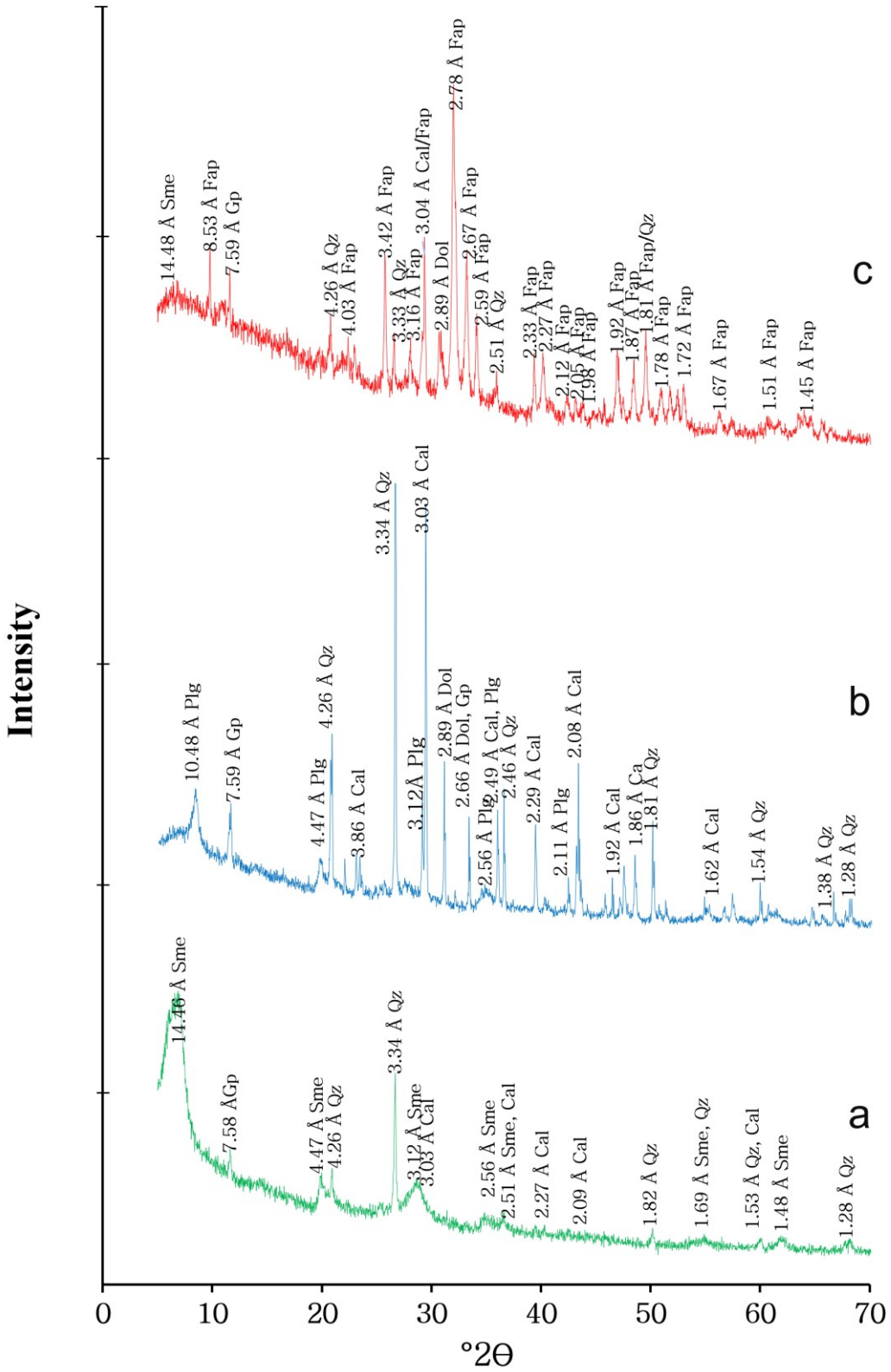

Figure 2a.

https://doi.org/10.1180/clm.2024.10 Published online by Cambridge University Press

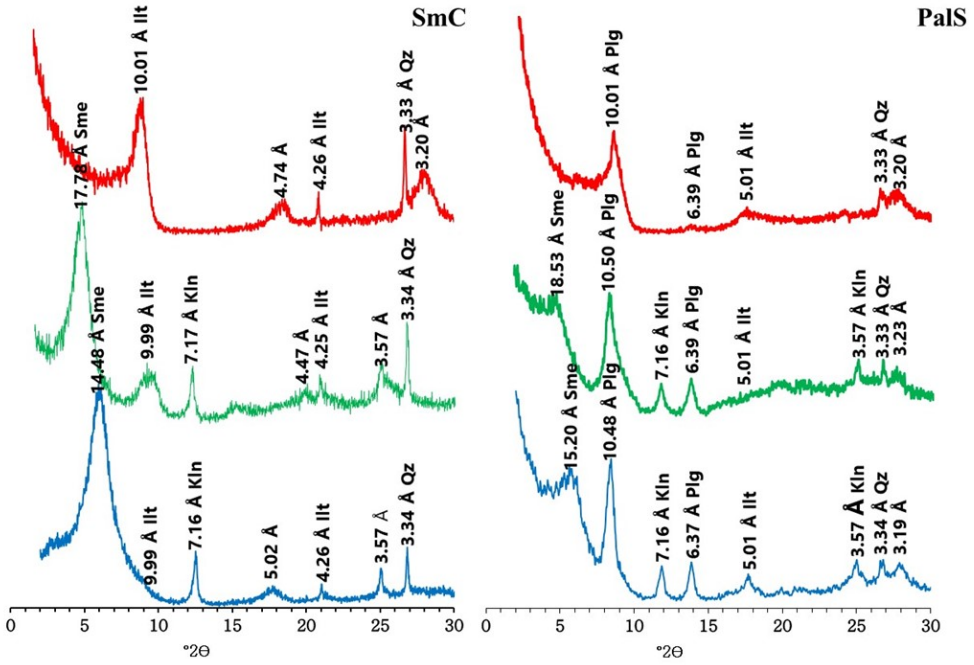

Figure 2b.

https://doi.org/10.1180/clm.2024.10 Published online by Cambridge University Press

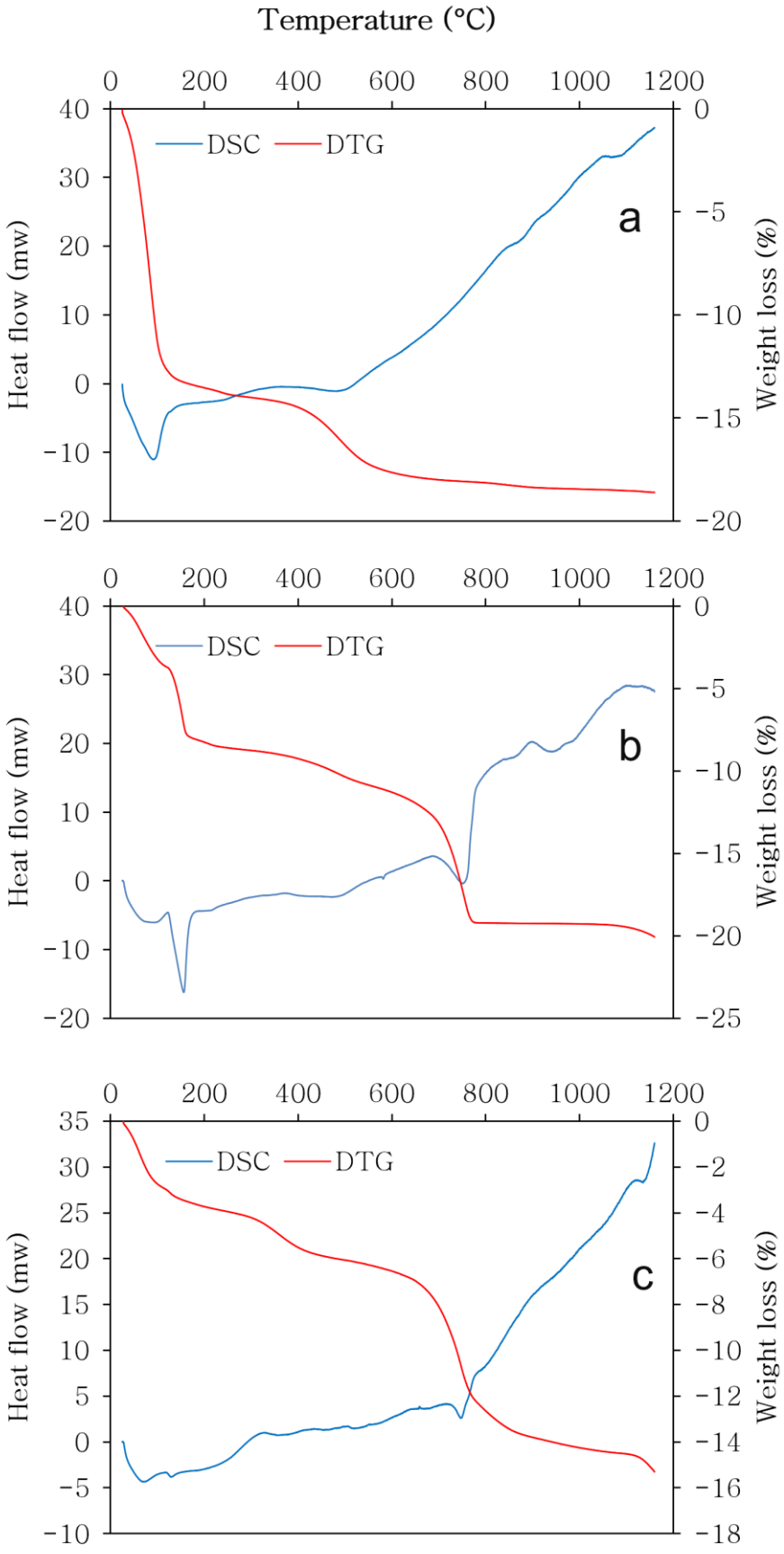

https://doi.org/10.1180/clm.2024.10 Published online by Cambridge University Press

Figure 3.

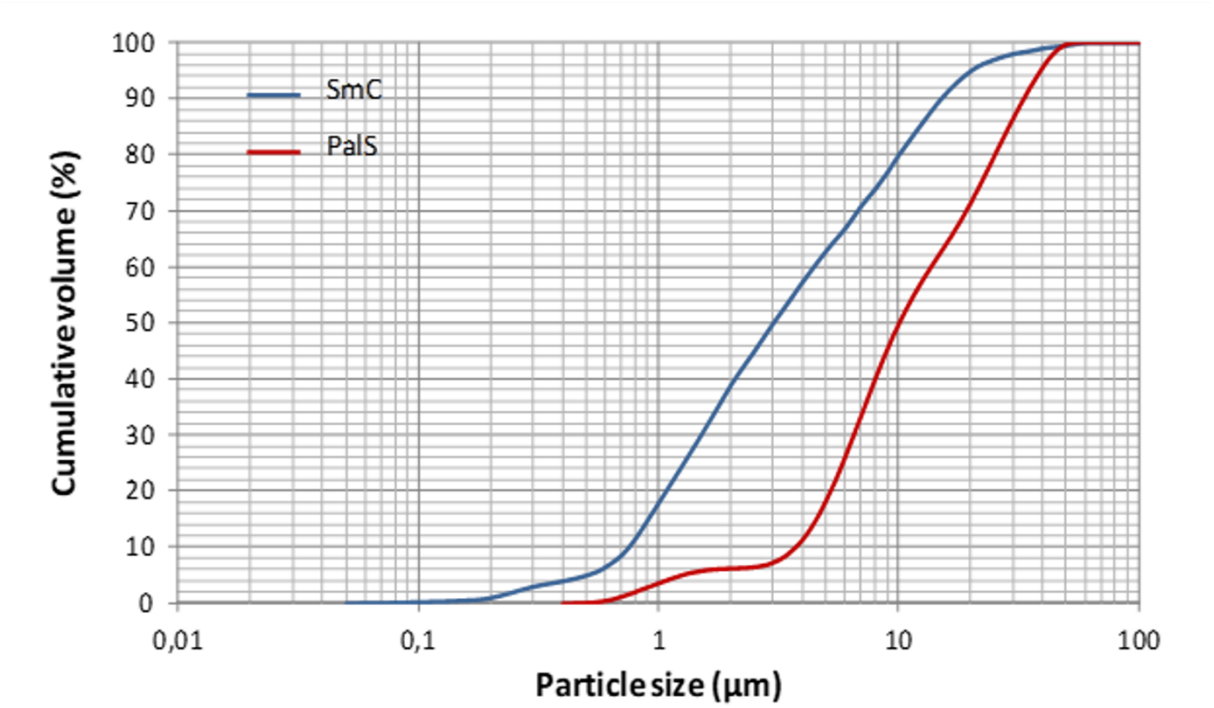

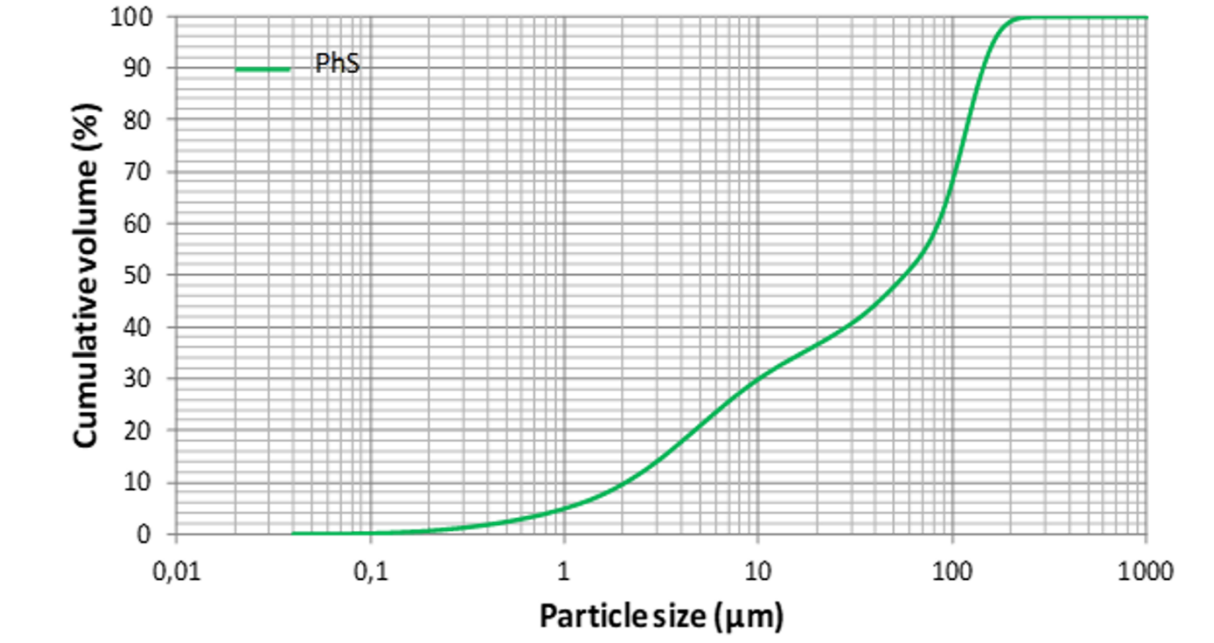

Figure 4.

https://doi.org/10.1180/clm.2024.10 Published online by Cambridge University Press

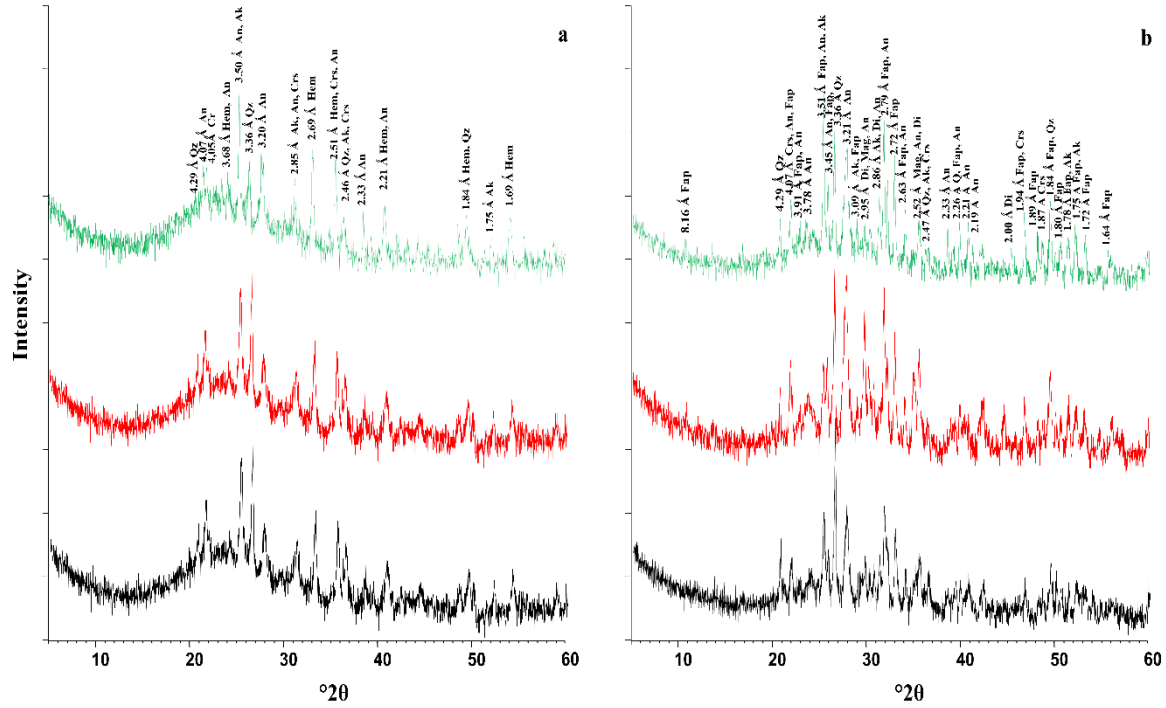

Figure 5.

Firing Temperature (°C) Formulation	1100	1125	1150
M1			
M2			

Figure 6.

https://doi.org/10.1180/clm.2024.10 Published online by Cambridge University Press

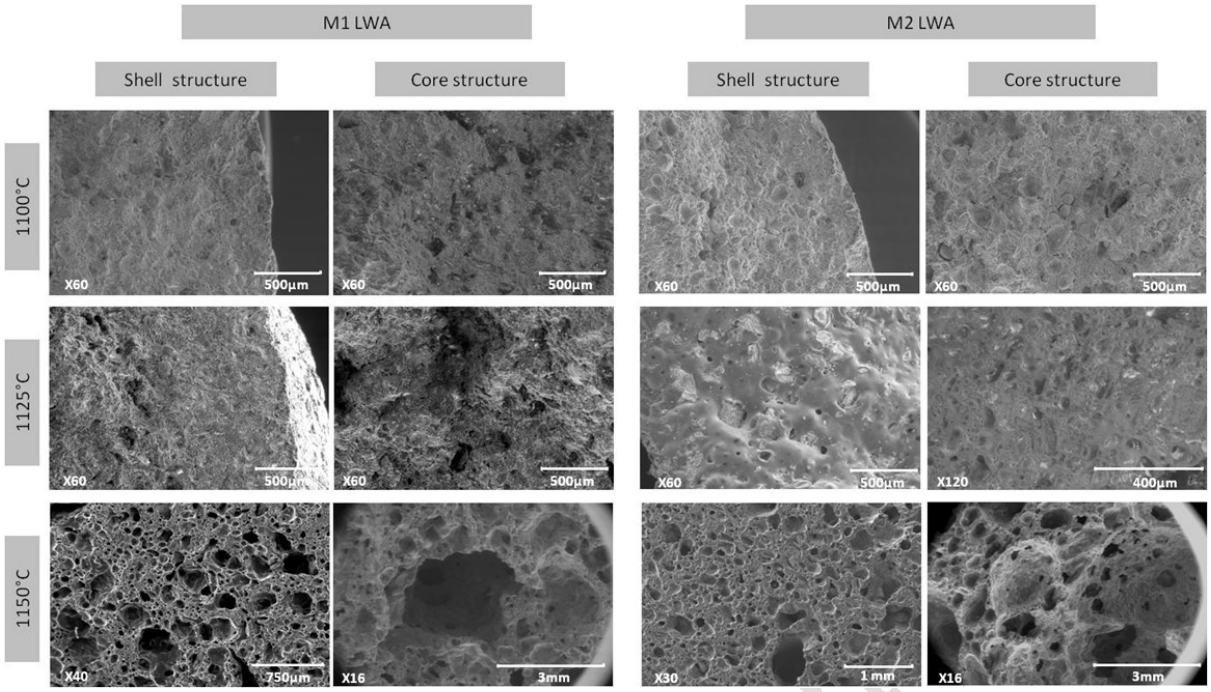

Figure 7.

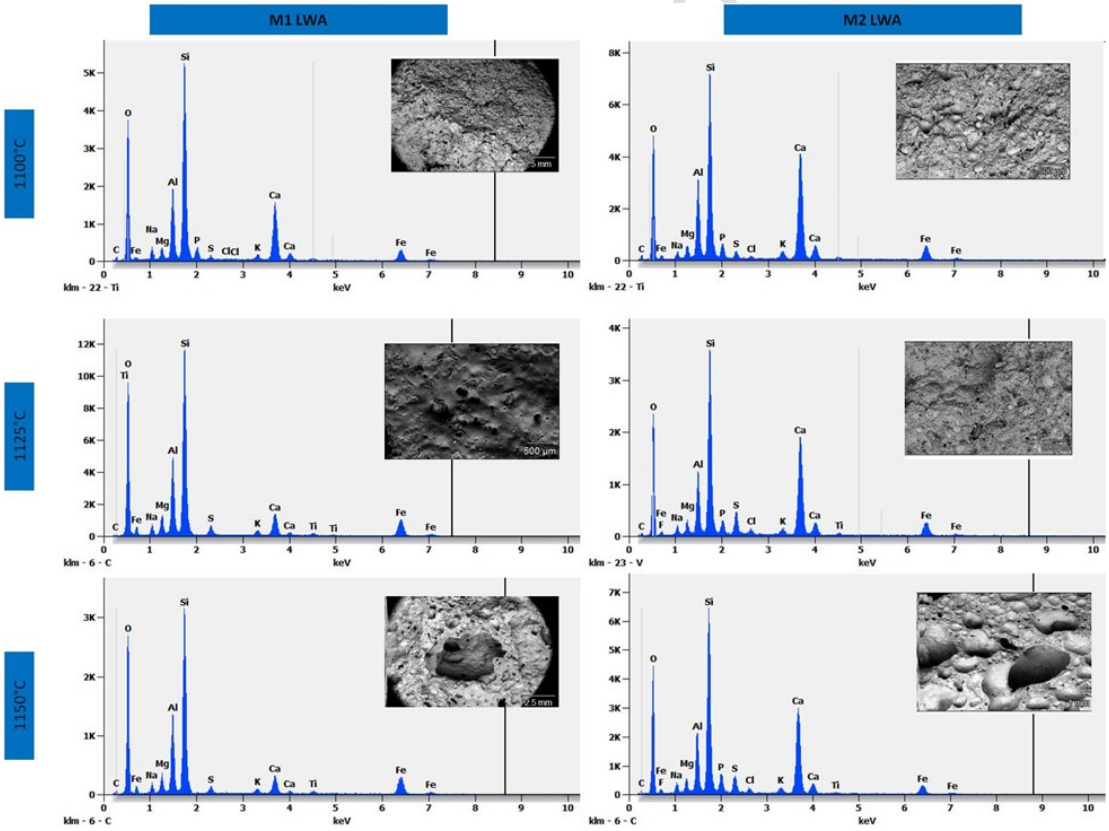

Figure 8.

https://doi.org/10.1180/clm.2024.10 Published online by Cambridge University Press

M1 LWA

1100°C

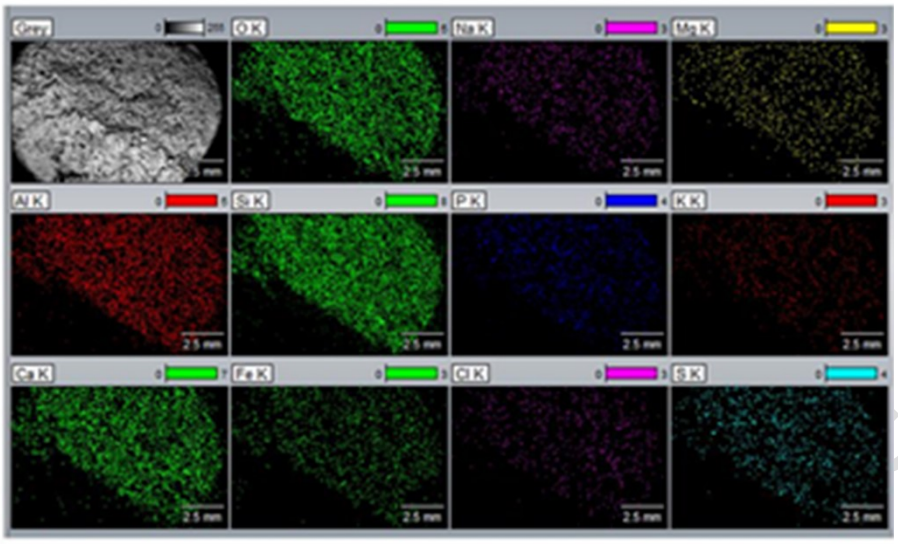

1125°C

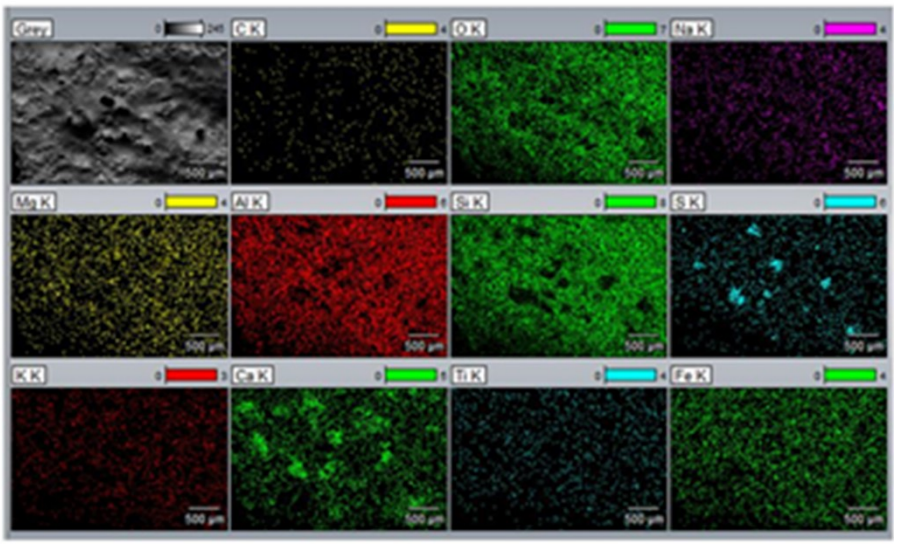

1150°C

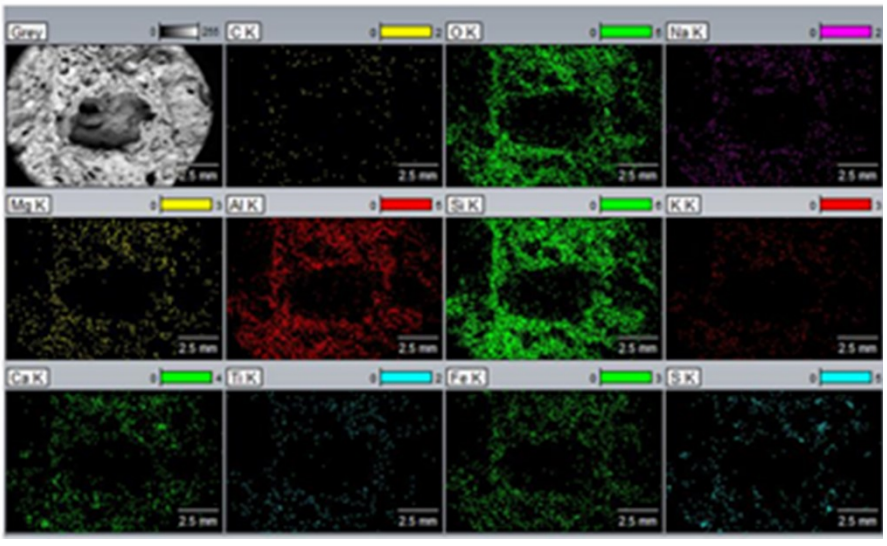

https://doi.org/10.1180/clm.2024.10 Published online by Cambridge University Press

Figure 9a

https://doi.org/10.1180/clm.2024.10 Published online by Cambridge University Press

M2 LWA

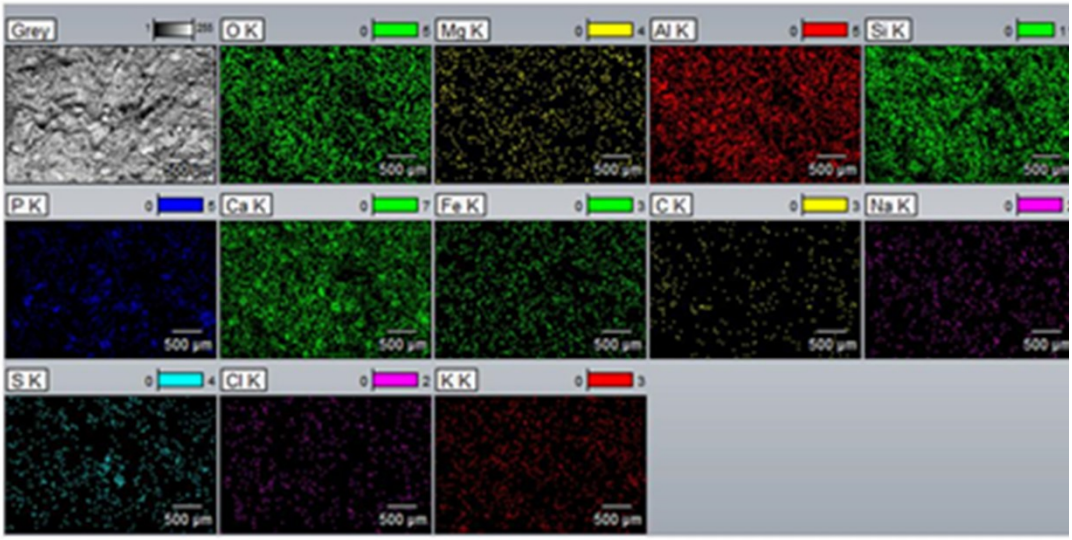

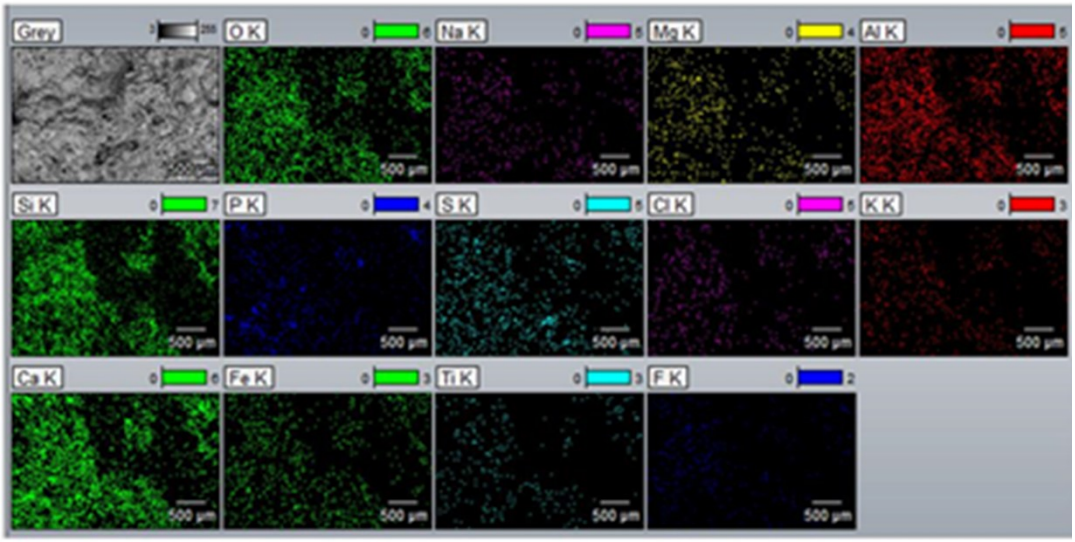

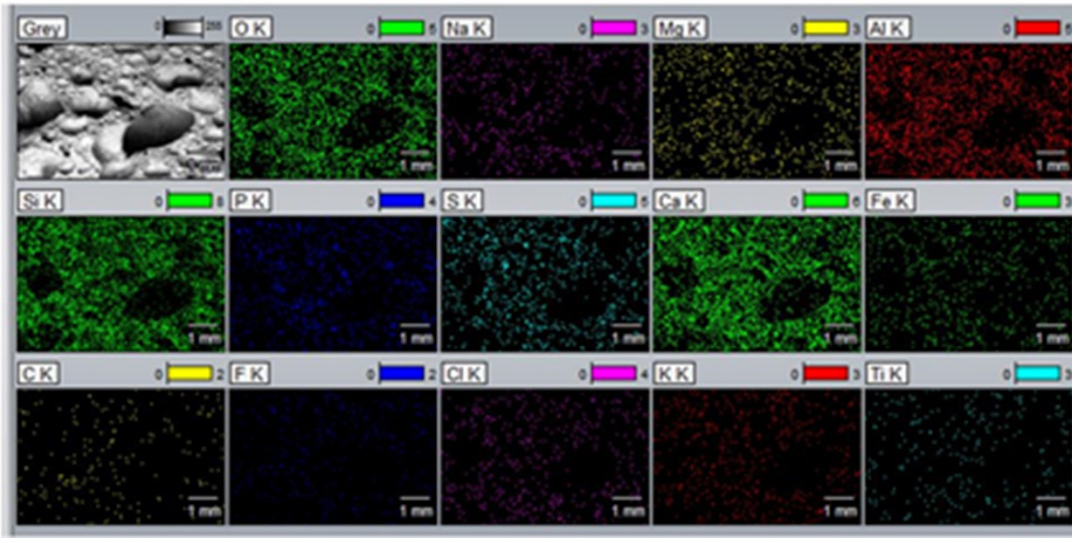

https://doi.org/10.1180/clm.2024.10 Published online by Cambridge University Press

Figure 9b.

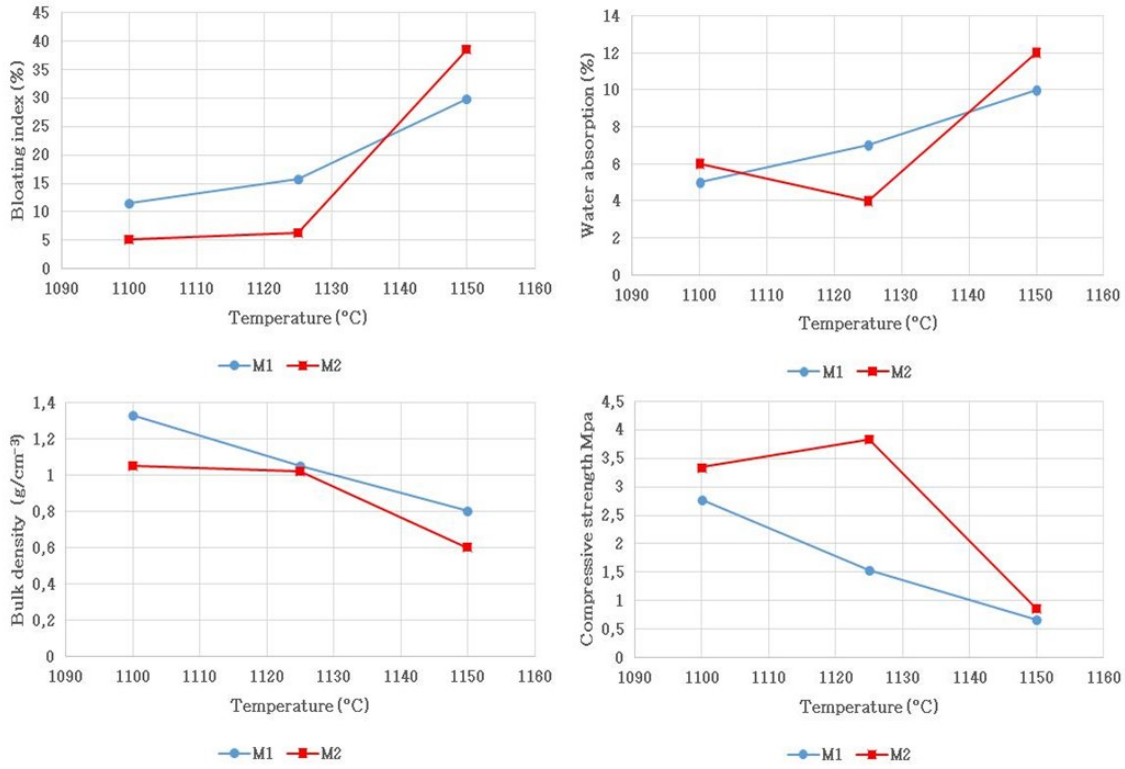

Figure 10.

https://doi.org/10.1180/clm.2024.10 Published online by Cambridge University Press